A multi-parameter system for real-time monitoring of landslide activity

Marco Pilz[1], Stefano Parolai[2], Tobias Boxberger[2]

(1) Swiss Seismological Service, ETH Zurich

(2) Helmholtz Center Potsdam – GFZ German Research Center for Geosciences

19 November 2015

Landslide hazard and risk

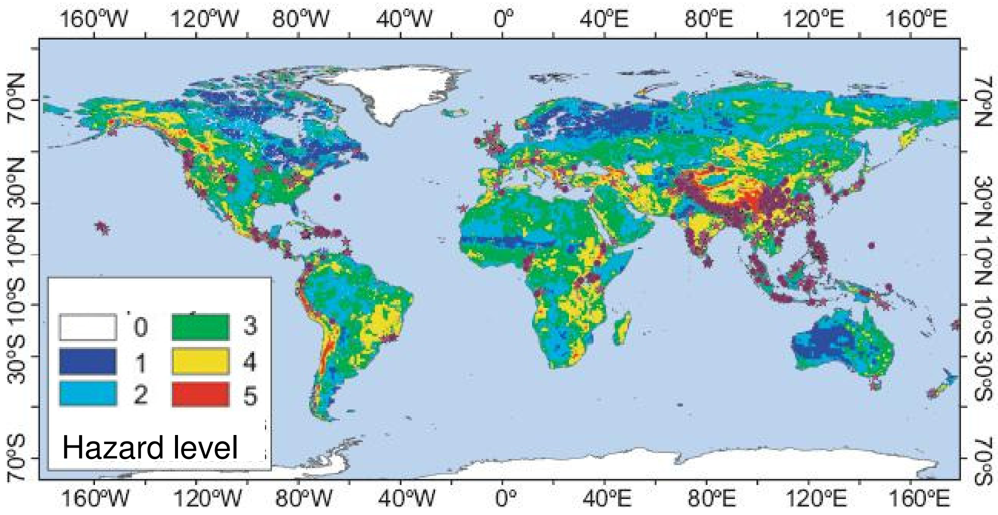

Landslide hazard

Petley et al. (2012)

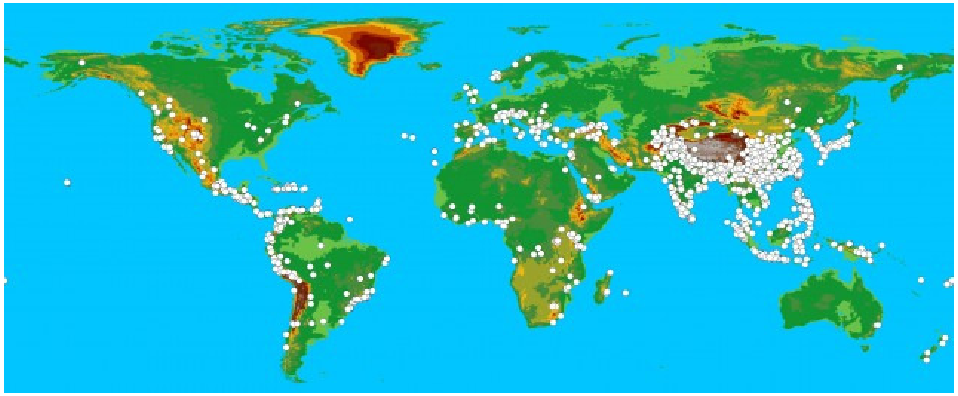

Almost 40,000 losses caused by landslides 2004-2010

Petley et al. (2012)

Current landslide monitoring systems

- LIDAR
- Photogrametic techniques
- Ground-based geodetic techniques like
  - Extensometers
  - Inclinometers
  - Strainmeters
  - Pore water pressure measurements / piezometers
  - Tiltmeters
  - Electronic Distance Measurement (EDM) instruments
  - Three-dimensional positioning systems with electronic theodolites

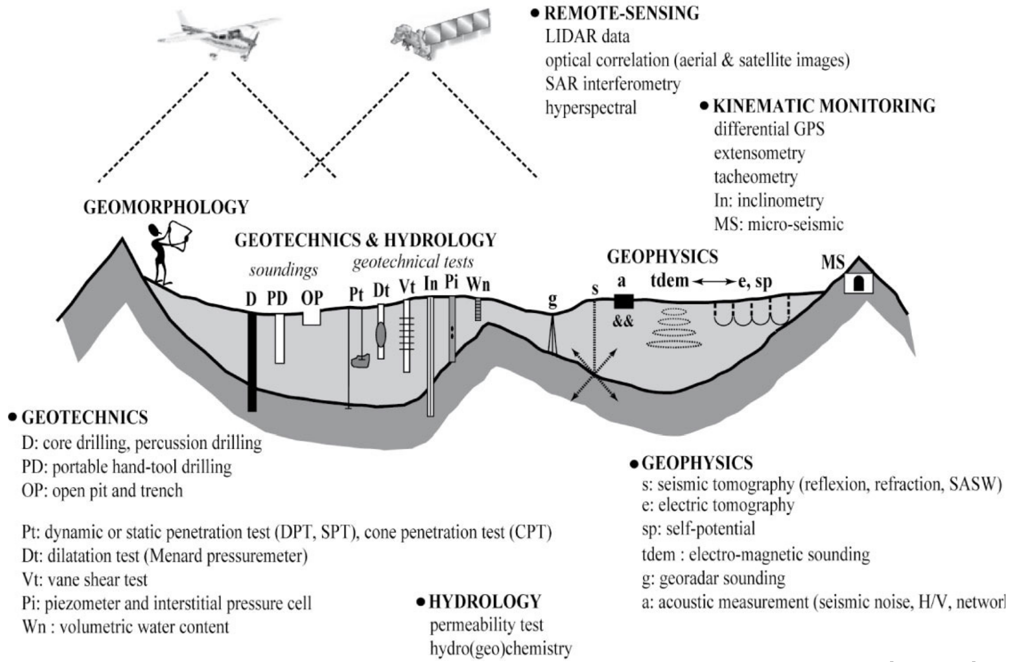

OMIV (2013)

Current landslide monitoring systems

Method of measurement	Displacement parameter	Distance between points	Typical accuracy
Metal tape or invar wire	Distance	< 30 m	0.5 mm / 30 m
Fixed wire extensometer	Distance	< 10 - 80 m	0.3 mm / 30 m
Inclinometer	Elevation angle	± 10º	± (5-10 mm ± 1-2 ppm)
Triangulation Trilateration	Dx, Dy, Dh	< 300 – 1000 m	2 – 10 mm
Traverses			
Robotic total station			
Precise geometric leveling			Km
Electromagnetic Distan Measurement			1-5 ppm)
Terrestrial Photogramm			
Aerial Photographs			
GPS L1/L2 static	Dx, Dy, Dh	[illegible] < 1-2 KM	[illegible] ppm) ± (1-3 mm ± 2ppm)
RTK DGPS	Dx, Dy, Dh	Variable	± (5 mm ± 2 ppm)
Continuous operating GPS	Dx, Dy, Dh	Variable	± 2 – 3 mm

All methods have their own advantages and disadvantages

There is the need for a combined and improved approach for **real-time** (and **remote**) **monitoring** of slope stability and landslide early warning

Savvaidis (2003)

Multi parameter early warning system

Technical Data	
Size	from 100 x 160 x 60 to 220 x 140 x 70 mm
Weight	from 0.75 to 2 kg
2 x WLAN	2.4 GHz / 5.0 GHz
Power Supply	5V DC
ADC	3 or 6 x ADC (24Bit)
Sensors	Ext. Seismometer, Camera Temp. Humidity GPS, ...,

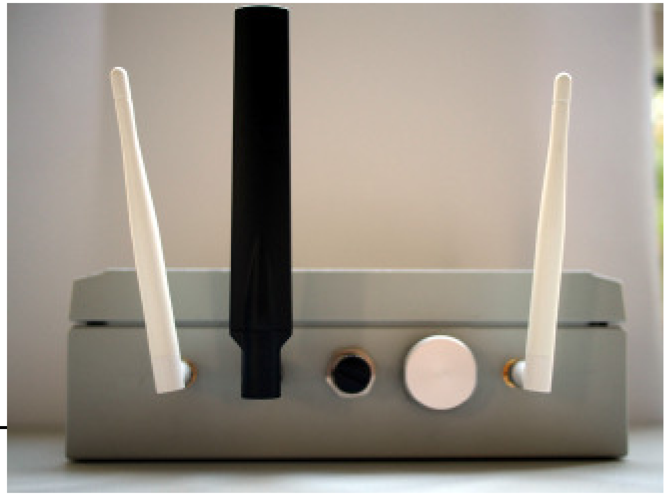

Multi parameter early warning system

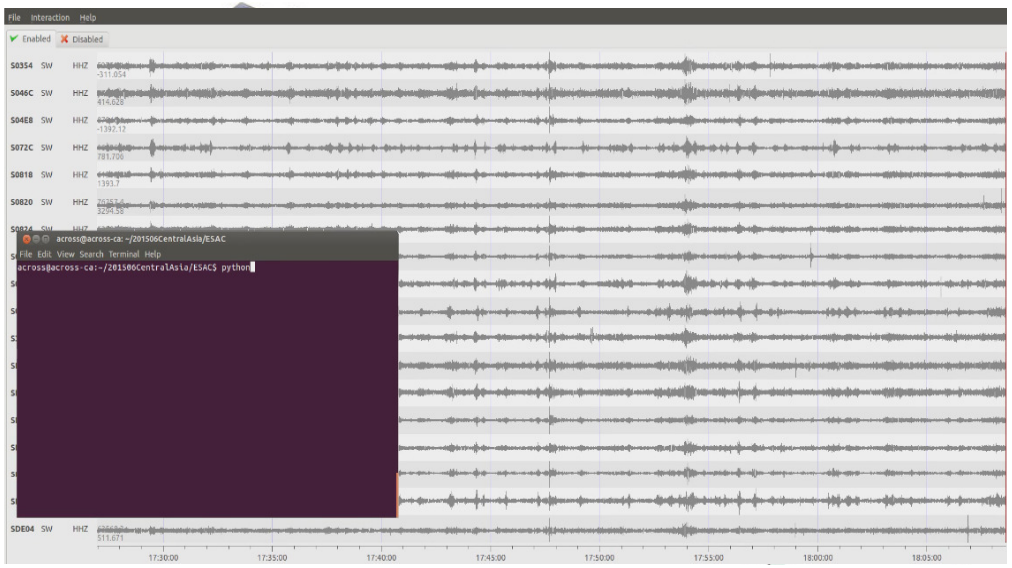

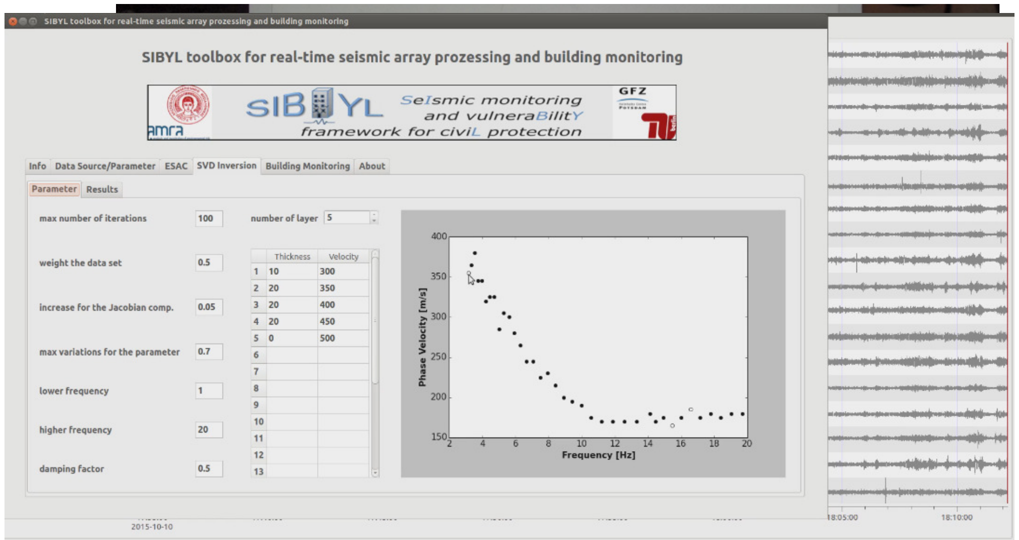

Sensor layer:

- standard strong motion and weak motion sensor
- broadband seismic sensors
- MEMS sensor including accelerometer and gyroscope
- camera
- temperature and humidity sensor
- low cost GNSS system

Communication layer:

- self organizing wireless network
- WLAN on the local scale
- UMTS

Continuous scenario update and calculations on the sensor level

Webinterface for configuration, network information and monitoring the status of acquisition

Seismic interferometry

Such seismic network are suitable for resolving subsoil heterogeneities making use of recent developments in seismic interferometry.

The reason for the success of this method is (at least in part) due to the striking maps of seismic velocities revealed by seismic noise interferometry.

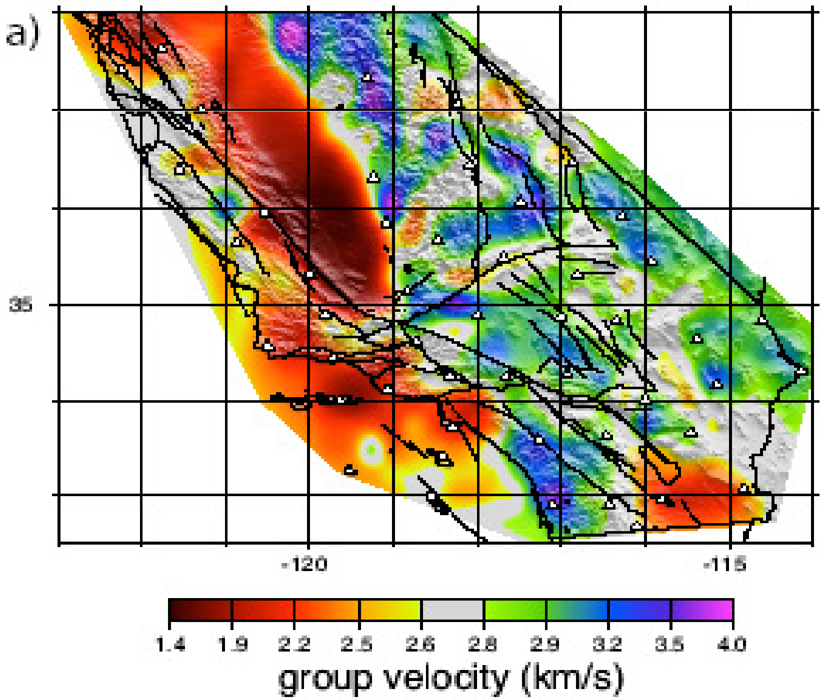

Map of 7.5s surface wave velocity obtained from correlation of seismic noise

Shapiro et al. (2005)

Our approach

Inversion procedure for imaging 3D shear-wave velocity structures on engineering scale using both Rayleigh and Love wave high frequency seismic noise

Seismic interferometry

For a diffusive wave field

$$\rho_z(r,\omega_0) = J_0\left(\frac{\omega_0}{c(\omega_0)} r\right)$$ Aki (1957)

Once the Rayleigh wave phase velocities are constrained by the analysis of the vertical component of motion, a similar iterative procedure can be implemented on the horizontal components of motion for the estimation of Love wave phase velocities

$$\rho_r(r,\omega_0) = \alpha\left[J_0\left(\frac{\omega_0 r}{c_R(\omega_0)}\right) - J_2\left(\frac{\omega_0 r}{c_R(\omega_0)}\right)\right] + (1-\alpha)\left[J_0\left(\frac{\omega_0 r}{c_L(\omega_0)}\right) + J_2\left(\frac{\omega_0 r}{c_L(\omega_0)}\right)\right]$$

$$\rho_t(r,\omega_0) = \alpha\left[J_0\left(\frac{\omega_0 r}{c_R(\omega_0)}\right) + J_2\left(\frac{\omega_0 r}{c_R(\omega_0)}\right)\right] + (1-\alpha)\left[J_0\left(\frac{\omega_0 r}{c_L(\omega_0)}\right) - J_2\left(\frac{\omega_0 r}{c_L(\omega_0)}\right)\right]$$

Metaxian et al. (1997)

Inversion problem

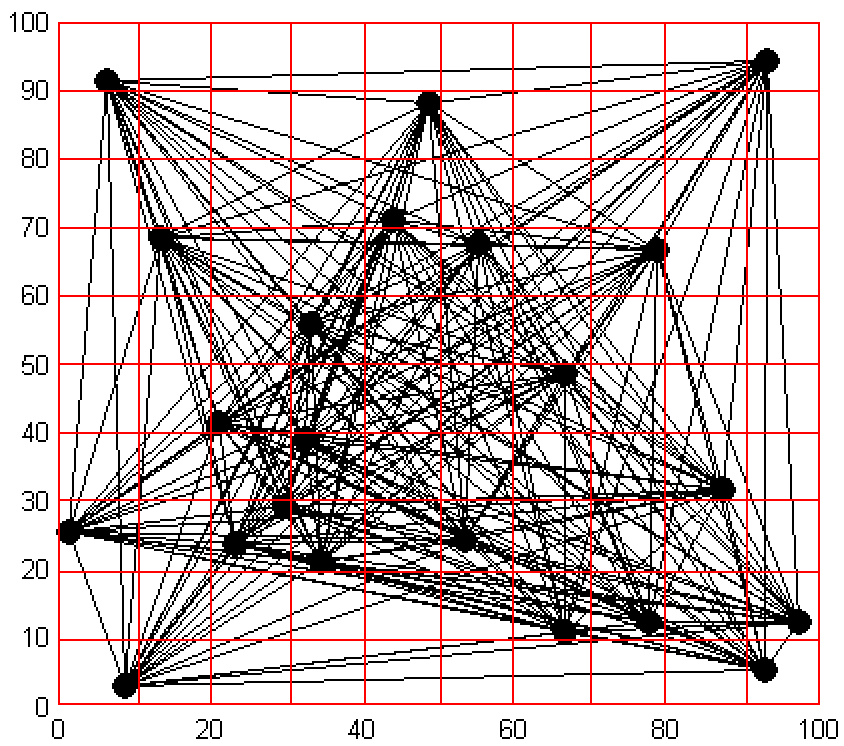

$$t = \int_L s \mathrm{d}l \qquad (1)$$

Linearization of the problem
→ Medium of interest is subdivided into reasonable number of smaller cells.

Iterative procedure for solving

$$\mathbf{W}\Delta\mathbf{t}^{(\mathbf{k})} = \mathbf{L}_2\Delta\mathbf{s}^{(\mathbf{k})} \qquad (2)$$

$\Delta\mathbf{t}$ is the vector of the normalized misfit between the observed and theoretical travel times
$\Delta\mathbf{s}$ is the vector of the normalized slowness modification
$\mathbf{W}$ is a weighting factor matrix

Data weighting

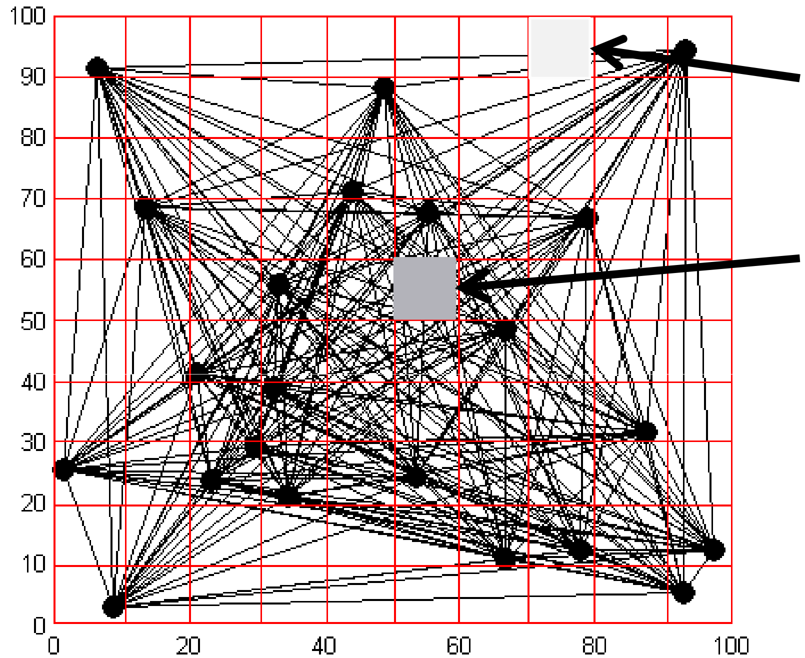

low weight: less well resolved

height weight: well resolved

Horizontal weights depend on number of rays, length and orientation for each sub-cell

Equation (2) was solved using SVD

$$\mathbf{\Delta s}^{(\mathbf{k})} = \mathbf{V}\mathbf{\Lambda}^{\varepsilon}\mathbf{U}^{\mathbf{T}}\mathbf{W}\mathbf{\Delta t}^{(\mathbf{k})} \quad (3)$$

where the factorization of **L** is **ULV**^{T} and the non-zero elements of the diagonal matrix are equal to $\lambda_{jj}/(\lambda_{jj}^{2}+\varepsilon^{2})$

One-step 3D imaging

Accounting for the frequency-dependent penetration depth of surface waves

Horizontal weighting

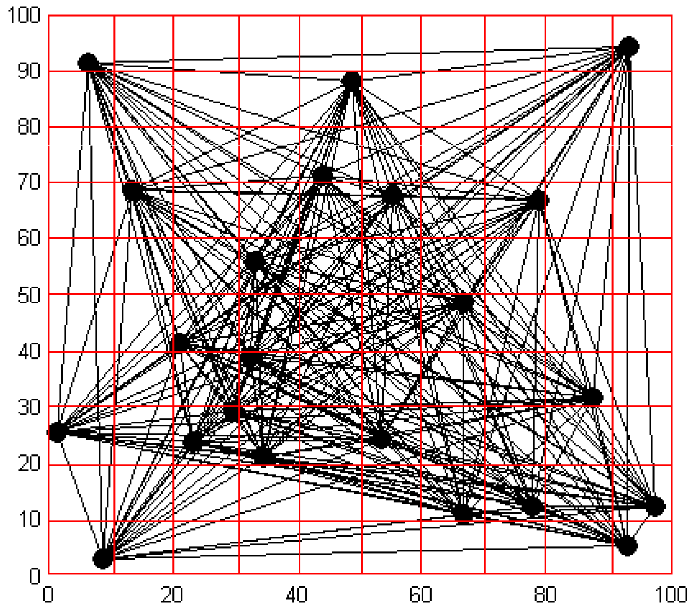

Vertical weighting

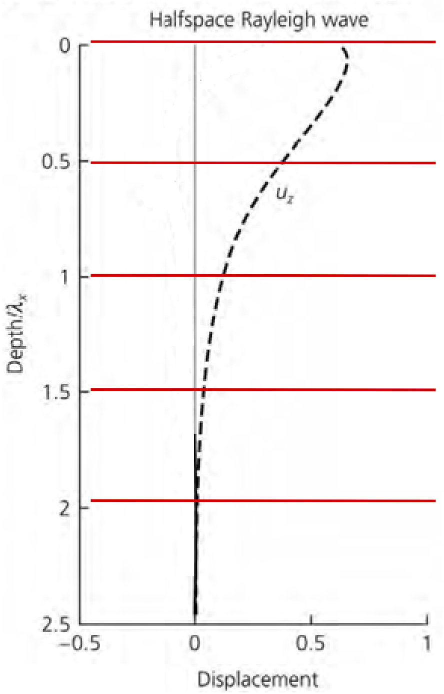

Data sensitivity kernels

The vertical weights are based on the analytical solution of displacement components for surface waves in a half space (Aki and Richards 1980, Borcherdt 2008).

Rayleigh waves

$$u_3(|\mathbf{z}|) = l e^{lk\mathbf{z}\cdot\mathbf{e}_z} - s e^{pk\mathbf{z}\cdot\mathbf{e}_z}$$

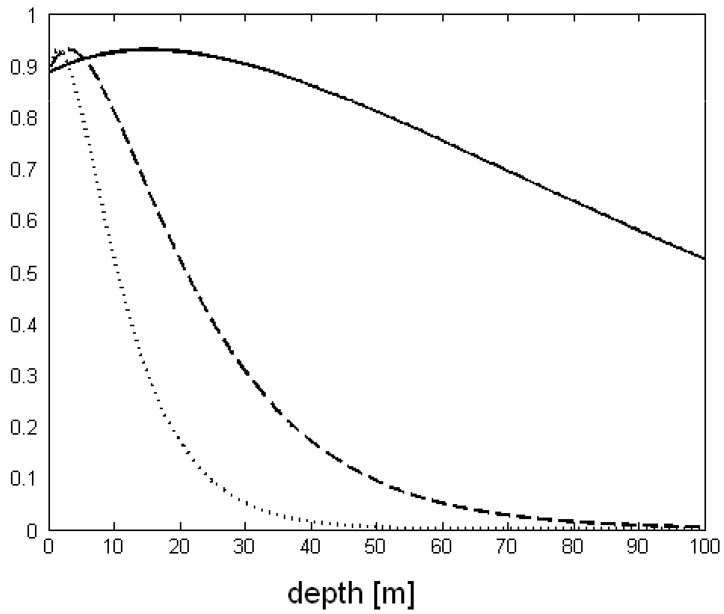

Love waves

$$u(|\mathbf{z}|) = \cos(\mathrm{Re}[B_n]\mathbf{z}\cdot\mathbf{e}_z) e^{i\frac{\omega}{c_{Love}}\mathbf{x}\cdot\mathbf{e}_x}$$

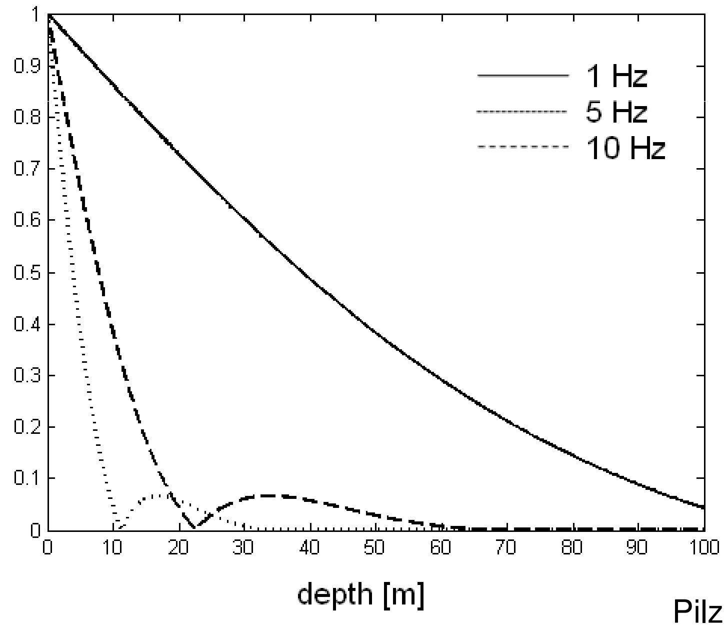

Pilz et al. (2012)

Since the vertical weights depend on the phase velocity they are updated after each iteration step.

Vertical weighting in case of significant topographic relief

wave length ≈ relief

$f_1 > f_2 > f_3$

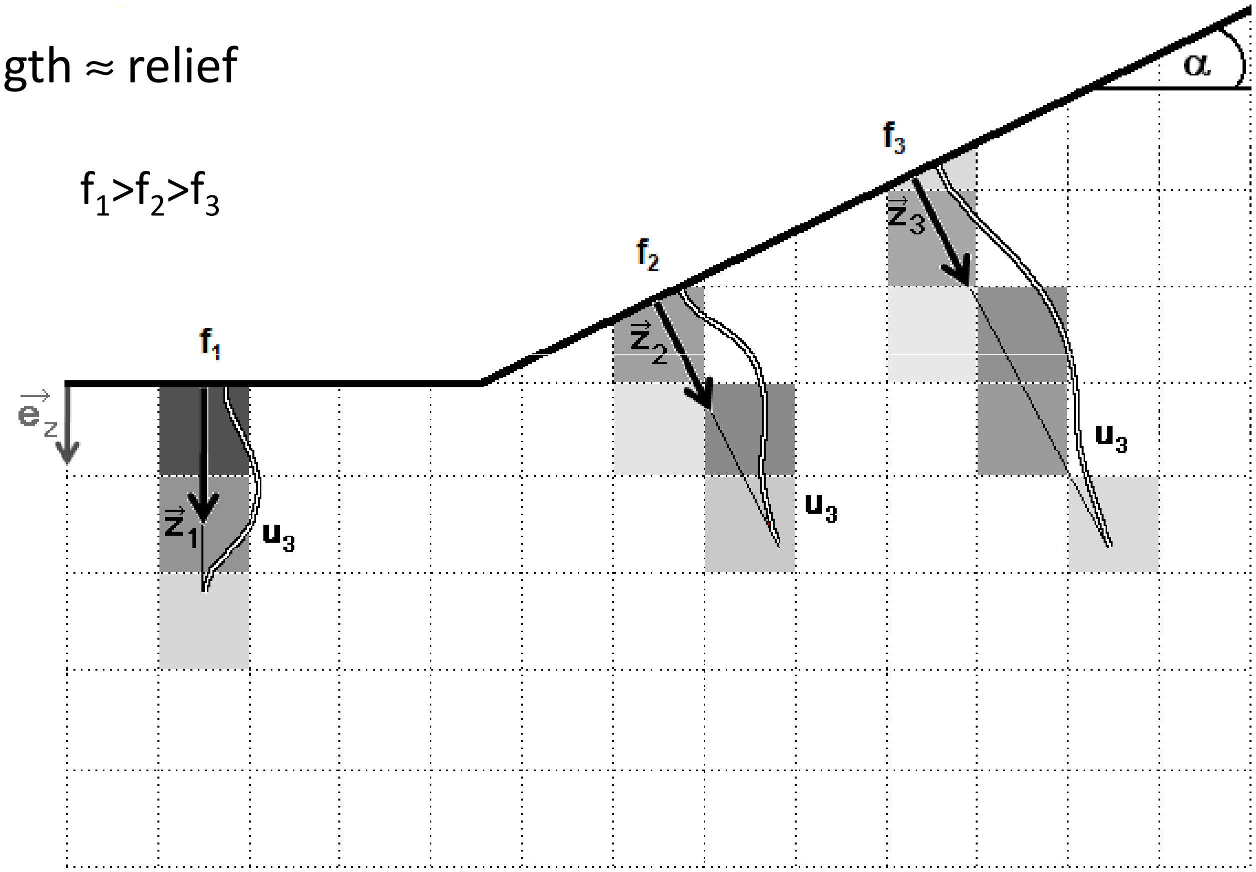

Pilz et al. (2013)

Deriving the 3D shear-wave velocity model

final weight W = horizontal weight * vertical weight for each cell

We solve $\mathbf{W\Delta t^{(k)} = L_2 \Delta s^{(k)}}$

For a given Rayleigh slowness **s** the shear-wave velocity can be calculated via

$$s = \frac{1}{c\,V_s}$$

with 0.9 < c < 0.95

Xia et al. (1999)

The Love wave phase velocity of one layer is related to shear-wave velocity through

$$\frac{\omega}{v_L} d_1 = \left(\sqrt{\frac{v_L^2}{v_{HS1}^2} - 1}\right)^{-1} \left(\arctan\left[\frac{\rho_2}{\rho_1}\frac{v_{HS2}^2}{v_{HS1}^2}\sqrt{1 - \frac{v_L^2}{v_{HS2}^2}}\Big/\sqrt{\frac{v_L^2}{v_{HS1}^2} - 1}\right] \mp n\pi\right)$$

Borcherdt (2008)

Imaging of a landslide

case study: Papan

Real-time imaging of a landslide

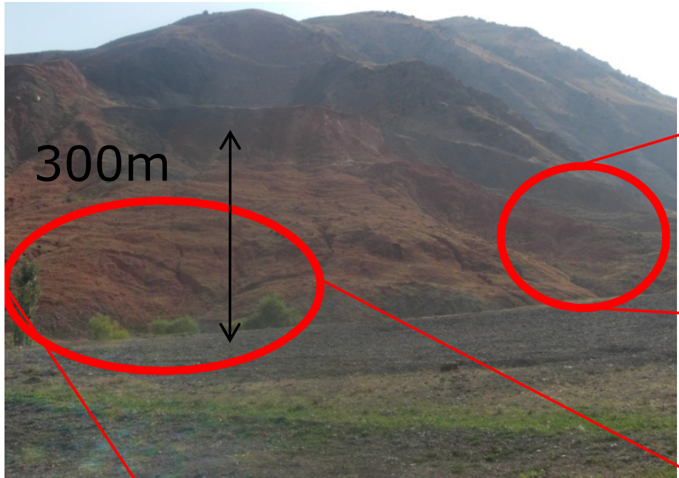

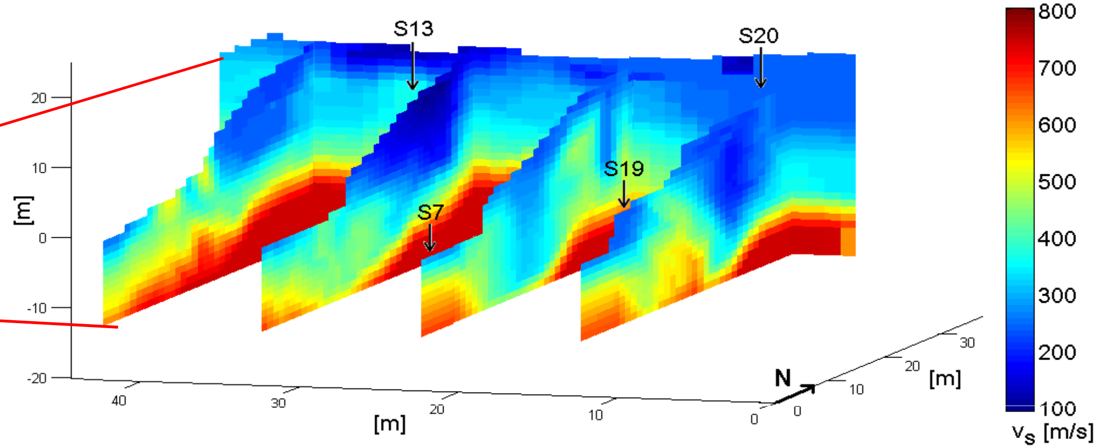

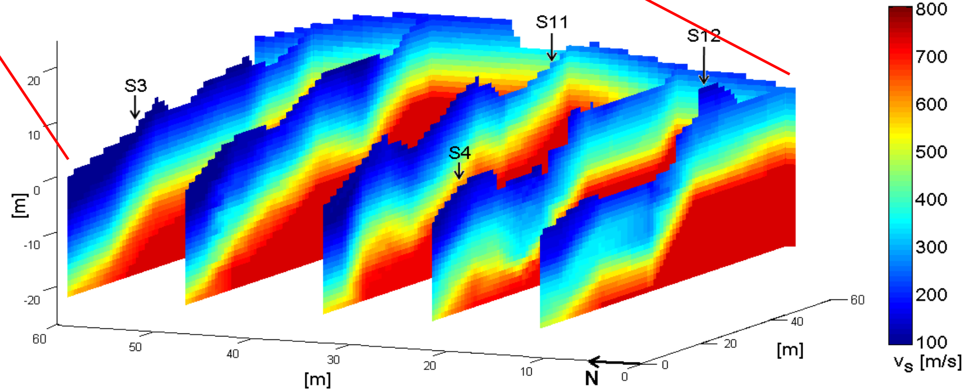

Pilz et al. (2014)

Real-time imaging of a landslide

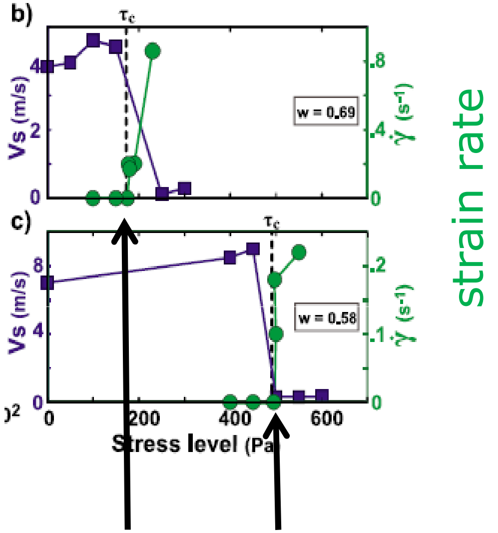

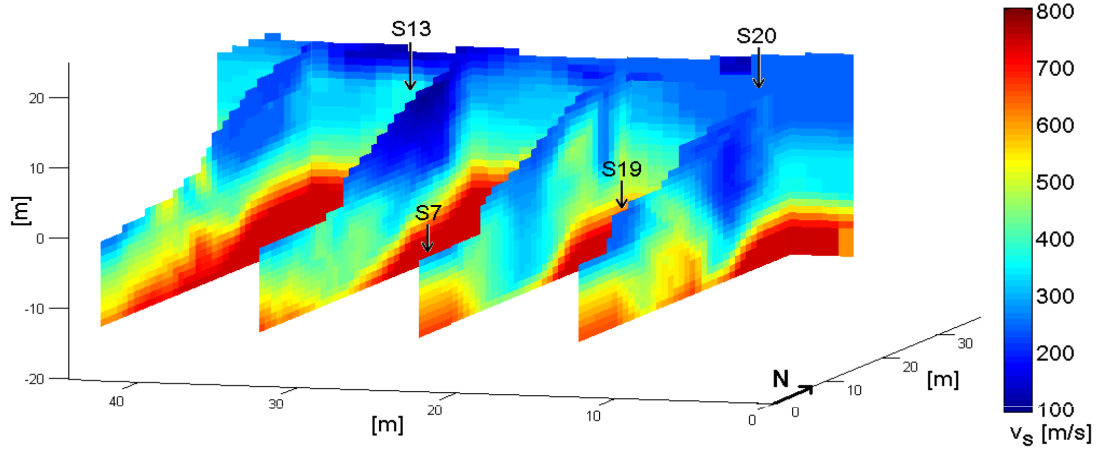

critical shear stress
for laboratory test
for clay

Mainsant et al. (2012)

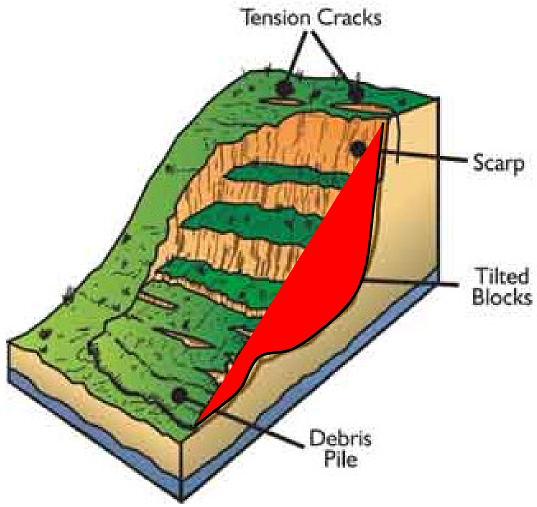

sliding
surface

Conclusions

- A multi-parameter early warning system allows several kinds of different sensors to be combined.
- Highly performing computing system is able to implement complex information integration and processing tasks at the sensor level in (almost) real-time.
- Seismic noise from a variety of sources produces diffuse wave fields which can be used to infer seismic velocities.
- A limited number of stations and recording times of some tens of minutes are sufficient for obtaining 3D local shear-wave velocity structures at reasonable computing times.